Supplementary information for "**Photochemical transformation of residential wood combustion emissions: dependence of organic aerosol composition on OH exposure**" by Hartikainen et al.

Table of Contents

Section S1 – Compounds assessed by online analyses **2**
Table S1: Gaseous compounds measured by FTIR 2
Table S2: Organic gaseous compounds identified by PTR-ToF-MS 3
Table S3: Polycyclic aromatic compounds included in the SP-HR-ToF-AMS HR-PAH analysis 4
Section S2 – OH exposure and external OH reactivity of RWC exhaust **5**
Figure S1: OH exposure during photochemical aging experiments 5
Figure S2: Contributions of the gaseous compounds measured by FTIR to the external OH reactivity of RWC exhaust 6
Section S3 – Primary emission **7**
Figure S3: Size distributions of diluted primary aerosol and condensation sinks in the PEAR OFR 7
Figure S4: Modified combustion efficiency 7
Figure S5: Average shares of the aromatic compound groups in unaged aerosol 8
Figure S6: Correlation between SP-HR-ToF-AMS and thermal-optical analyses 8
Table S4: Concentrations of primary gaseous emissions measured by FTIR. 9
Section S4 – Conditions in the PEAR OFR **10**
S4.1. Photochemical aging conditions 10
Table S5: Estimation equations used for determination of exposures 11
Table S6: Average radical exposures in the PEAR OFR 11
Figure S7: OHR_{ext} in the PEAR OFR and riskiness of the aging conditions 12
Figure S8: Estimated fate of RO_2 in the PEAR OFR 12
Figure S9: Relative shares and atmospheric relevance of reaction pathways 13
Table S7: Absorption cross sections and reaction rates of some of the major VOCs from RWC 13
Figure S10: Relative shares of degredation pathways for benzene and toluene 14
S4.2 Fate of low-volatility organic compounds in the PEAR OFR 15
Figure S11: Relative shares of the LVOC fates 16
Section S5 – Transformation of the particulate phase **17**
Figure S12: Particle number enhancement ratios 17
Table S8: Chemical composition of the PM 18
Figure S13: Relationship between photochemical age and OA composition 19
Figure S14: Compounds analysed by IDTD-GC-ToFMS displayed in the OS_C-n_C space 20
Figure S15: Timeseries of the concentrations and average carbon oxidation states of particulate OA. 20
Figure S16: Spectra of the PMF factors 21
Figure S17: Correlations between PMF factors and tracers 21
S5.1 In-situ derivatisation and thermal desorption - gas-chromatography - time-of-flight mass spectrometry 22
Table S9: Isotopically labelled internal standards used for polar compounds 22
Table S10: Isotopically labelled internal standards for nonpolar compounds 23
Table S11: Secondary concentrations of compounds measured by IDTD-GC-ToFMS. Attached as a .xlsx file 23
Table S12: Pearson correlation coefficients between the particulate OA constituents 24
References **25**

Section S1 – Organic species assessed by online analyses

Table S1: Gaseous compounds measured by FTIR and their reaction rates with OH (k_{OH}; NIST Kinetics Database, Manion et al., 2015).

Compound	Formula	OGC group	CAS	Range	unit	k_{OH} [cm^3 $molec.^{-1}$ s]
Water vapor	H_2O		7732-18-5	30	vol-%	2.10E-16
Carbon dioxide	CO_2		124-38-9	25	vol-%	
Carbon monoxide	CO		630-08-0	5000	ppm	2.41E-13
				2	vol-%	
Nitrous oxide	N_2O		10024-97-2	200	ppm	2.01E-16
Nitrogen monoxide	NO		10102-43-9	1000	ppm	1.00E-11
Nitrogen dioxide	NO_2		19192-44-0	200	ppm	1.06E-11
Sulfur dioxide	SO_2		7446-09-5	1000	ppm	1.31E-12
Carbonyl sulfide	COS		483-58-1	100	ppm	1.96E-15
Ammonia	NH_3		7664-41-7	500	ppm	1.57E-13
Hydrogen chloride	HCl		7647-01-0	200	ppm	7.86E-13
Hydrogen cyanide	HCN		74-90-8	100	ppm	3.13E-14
Hydrogen fluoride	HF		7664-39-3	100	ppm	
Methane	CH_4		74-82-8	1000	ppm	6.28E-15
Ethane	C_2H_6	Alkane	74-84-0	200	ppm	2.41E-13
Propane	C_3H_8	Alkane	74-98-6	200	ppm	1.10E-12
Butane	C_4H_{10}	Alkane	106-97-8	200	ppm	2.33E-12
Pentane	C_5H_{12}	Alkane	109-66-0	200	ppm	3.80E-12
Hexane	C_6H_{14}	Alkane	110-54-3	200	ppm	5.20E-12
Heptane	C_7H_{16}	Alkane	142-82-5	200	ppm	6.76E-12
Octane	C_8H_{18}	Alkane	111-65-9	200	ppm	7.43E-12
Acetylene	C_2H_2	Unsaturated	75-86-2	200	ppm	7.75E-13
Ethylene	C_2H_4	Unsaturated	74-85-1	200	ppm	8.51E-12
Propene	C_3H_6	Unsaturated	115-07-1	200	ppm	3.01E-11
1,3-Butadiene	C_4H_6	Unsaturated	106-99-0	200	ppm	6.93E-11
Benzene	C_6H_6	Aromatic	71-43-2	200	ppm	1.28E-12
Toluene	C_7H_8	Aromatic	108-88-3	200	ppm	6.16E-12
m-Xylene	C_8H_{10}	Aromatic	108-38-3	200	ppm	2.45E-11
o-Xylene	C_8H_{10}	Aromatic	95-47-6	200	ppm	1.47E-11
p-Xylene	C_8H_{10}	Aromatic	106-42-3	200	ppm	1.52E-11
1,2,3-Trimethylbenzene	C_9H_{12}	Aromatic	526-73-8	200	ppm	2.89E-11
1,2,4-Trimethylbenzene	C_9H_{12}	Aromatic	95-63-6	200	ppm	3.16E-11
1,35-Trimethylbenzene	C_9H_{12}	Aromatic	106-42-3	200	ppm	5.98E-11
Formic acid	CH_2O	Oxygenated	64-18-6	200	ppm	4.50E-13
Acetic acid	$C_2H_4O_2$	Oxygenated	64-19-7	200	ppm	6.69E-13
Formaldehyde	CHOH	Oxygenated	50-0-0	200	ppm	9.38E-12
Acetaldehyde	C_2H_4O	Oxygenated	75-07-0	200	ppm	1.63E-11
Methanol	CH_4O	Oxygenated	67-56-1	500	ppm	9.28E-13
Ethanol	C_2H_6O	Oxygenated	64-17-5	500	ppm	3.24E-12
Propanol	C_3H_8O	Oxygenated	71-23-8	500	ppm	5.82E-12

Table S2: Organic gaseous compounds identified from the RWC exhaust by PTR-ToF-MS and the applied reaction rates with H_3O^+ (Cappellin et al., 2012).

m/z	Ion	Suggested compound	k
Aliphatic hydrocarbons			
53.04	C4H4-H+	Butenyne	2.00
55.06	C4H6-H+	1,3-Butadiene	1.80
67.06	C5H6-H+	1,3-cyclopentadiene	1.83
69.07	C5H8-H+	Isoprene	1.95
97.11	C7H12-H+	Cycloheptene	2.00
109.10	C8H12-H+	e.g. Cyclohexene, 4-ethenyl-	2.00
137.13	C10H16-H+	Monoterpenes	2.42
Aromatic hydrocarbons			
79.05	C6H6-H+	Benzene	1.93
93.07	C7H8-H+	Toluene	2.08
105.07	C8H8-H+	Styrene	2.27
107.09	C8H10-H+	Xylene, ethylbenzenes	2.26
119.08	C9H10-H+	e.g. Indane, methylstyrene	2.00
121.10	C9H12-H+	C3 benzenes; e.g. Cumene	2.40
129.07	C10H8-H+	Naphthalene	2.45
143.09	C11H10-H+	Methylnaphthalene	2.71
155.08	C12H10-H+	e.g. Acenaphthene	2.82
167.08	C13H10-H+	Fluorene	2.88
Phenolic compounds			
95.05	C6H6O2-H+	Phenol	2.20
109.07	C7H8O-H+	Cresols	3.20
111.04	C6H6O2-H+	Benzenediols	2.00
123.08	C8H10O-H+	Dimethylphenol	2.00
125.06	C7H8O2-H+	Guaiacol	2.00
139.04	C7H6O3-H+	e.g. Salicylic acid	2.00
139.08	C8H10O2-H+	Creosol, Trosol	2.00
153.07	C8H8O3-H+	e.g. Methoxy-benzoic acid	2.00
Furanoic compounds			
69.03	C4H4O-H+	Furan	1.70
83.05	C5H6O-H+	Methylfurans	2.00
85.03	C4H4O2-H+	Furanone	2.00
97.03	C5H4O2-H+	Furfural	3.95
97.07	C6H8O-H+	Dimethyl- & ethyl furan	2.00
99.04	C5H6O2-H+	Furfuryl alcohol	2.00
119.05	C8H6O-H+	Benzofuran	2.00
125.02	C6H4O3-H+	2,5-Furandicarboxaldehyde	2.00
127.04	C6H6O3-H+	5-Hydroxymethylfurfural	2.00
Nitroaromatics			
140.03	C6H5NO3-H+	Nitrophenols	2.00
154.06	C7H7NO3-H+	e.g. Nitrocresol	2.00
Other oxygenated aromatics			
107.05	C7H6O-H+	Benzaldehyde	3.73
109.03	C6H4O2-H+	Benzoquinones	1.99
121.07	C8H8O-H+	E.g. Acetophenone	3.36
123.04	C7H6O2-H+	Benzoic acid	2.68
133.06	C9H8O-H+	e.g. Cinnamic acid	2.00
135.04	C8H6O2-H+	e.g. Isophthalaldehyde, phenylglyoxal	2.00
135.08	C9H10O-H+	e.g. 4-Ethylbenzaldehyde	2.00
137.06	C8H8O2-H+	e.g. Benzeneacetic acid	2.00
141.05	C7H8O3-H+		2.00
147.06	C9H6O2-H+	e.g. Coumarin	2.00
149.02	C8H4O3-H+	Phthalic anhydride	2.00
151.04	C8H6O3-H+	e.g. Benzoylformic acid	2.00
151.08	C9H10O2-H+	e.g. Hydrocinnamic acid	2.00
151.11	C10H14O-H+	e.g. Verbenone	2.00
159.04	C10H6O2-H+	Naphthalenedione	2.00
163.04	C9H6O3-H+		2.00
169.07	C12H8O-H+	e.g. dibenzofuran	2.00
CHN			
42.04	C2H3N-H+	Acetonitrile	3.90
54.04	C3H3N-H+	Propenenitrile	2.00
56.05	C3H5N-H+	e.g. Propanenitrile	2.00
68.05	C4H5N-H+	e.g. Pyrrole	2.38
70.07	C4H7N-H+	e.g. Butanenitrile	2.00
84.09	C5H9N-H+	e.g. Pentanenitrile	2.00
100.08	C5H9N3-H+		2.00
104.05	C7H5N-H+	Benzonitrile	2.00
118.06	C8H7N-H+	Indole	2.00

m/z	Ion	Suggested compound	k
Carbonyls - primary			
45.03	C2H4O-H+	Acetaldehyde	3.07
55.02	C3H2O-H+	2-propynal	2.00
57.03	C3H4O-H+	Acrolein	3.49
71.02	C3H2O2-H+	Propiolic acid	2.00
71.05	C4H6O-H+	Methyl vinyl ketone, methacrolein	3.20
73.03	C3H4O2-H+	2-Propenoic acid	2.60
75.04	C3H6O2-H+	Hydroxy-2-propanone	2.33
83.01	C4H2O2-H+	3-Cyclobutene-1,2-dione	2.00
85.07	C5H8O-H+	e.g. Pentenal	2.00
87.05	C4H6O2-H+	e.g. 2,3- butadione	1.70
99.08	C6H10O-H+	e.g. Hexenal	3.74
101.06	C5H8O2-H+	e.g. Acetylacetone	2.93
103.04	C4H6O3-H+	Acetic anhydride	2.00
103.08	C5H10O2-H+	e.g. Methyl-butanoic acid	2.00
117.02	C4H4O4-H+	Fumaric acid	2.00
117.06	C5H8O3-H+	e.g. Acetyloxypropanone	2.00
Carbonyls - secondary			
59.05	C3H6O-H+	Acetone, propanal	3.20
61.03	C2H4O2-H+	Acetic acid, glycolaldehyde	2.30
73.07	C4H8O-H+	2-butanone and 2-methylpropanal	3.12
77.02	C2H4O3-H+	Acetic acid, hydroxy-	2.00
89.03	C3H4O3-H+	E.g. Acetic acid anhydride with formic acid	2.00
89.06	C4H8O2-H+	Acetoin	4.23
99.01	C4H2O3-H+	Maleic anhydride	2.00
101.02	C4H4O3-H+	Succinic anhydride	2.00
105.04	C4H8O3-H+	e.g. Acetic acid, methoxy-	2.00
Other CHO			
47.05	C2H6O-H+	Ethanol	2.11
49.03	CH4O2-H+	Methyl peroxide or methanediol	2.00
63.04	C2H6O2-H+	ethanediol	1.47
77.05	C3H8O2-H+	e.g. Ethanol 2-methoxy- ; 1,3-Propanediol	3.50
81.04	C5H4O-H+	2,4-Cyclopentadiene-1-one	2.00
91.07	C4H10O2-H+	Butanediols	2.00
111.08	C7H10O-H+	e.g. Heptenedial or trimethylfuran	2.00
113.02	C5H4O3-H+	e.g. 2-furoic acid	2.00
113.06	C6H8O2-H+	eg. Methylcyclohexanone	2.00
115.04	C5H6O3-H+	e.g. Hydroxymethylfuranone	2.00
115.08	C7H10O2-H+		2.00
115.11	C7H14O-H+	e.g. Heptanal	2.83
117.09	C6H12O2-H+		2.00
127.08	C7H10O2-H+		2.00
139.11	C9H14O-H+		2.00
145.05	C6H8O4-H+	e.g. Dimethyl fumarate	2.00
157.08	C8H12O3-H+		2.00
CHNO			
44.01	CHNO-H+	Isocyanic acid	2.00
58.03	C2H3NO-H+	Methyl isocyanate	2.00
60.05	C2H5NO-H+	e.g. Acetamide	2.00
62.03	CH3NO2-H+	e.g. Nitromethane, methyl nitrite	2.00
70.03	C3H3NO-H+	e.g. Vinyl isocyanate	2.00
74.03	C2H3NO2-H+	e.g. Nitroethylene	2.00
74.06	C3H7NO-H+	Propanamide	2.00
84.05	C4H5NO-H+		2.00
86.03	C3H3NO2-H+	Acetic acid, cyano-	2.00
86.07	C4H7NO-H+	e.g. Methacrylamide	2.00
88.05	C3H5NO2-H+	Nitropropene	2.00
88.08	C4H9NO-H+		2.00
96.06	C5H5NO-H+	Pyridine-N-oxide	2.00
100.04	C4H5NO2-H+		2.00
112.05	C5H5NO2-H+		2.00
114.02	C4H3NO3-H+	Nitrofuran	2.00
114.06	C5H7NO2-H+	e.g. Ethyl cyanoacetate	2.00
120.05	C7H5NO-H+	e.g. Benzisoxazole	2.00
122.02	C2H3NO5 -H+	peroxyacetyl nitrate	2.00
122.07	C7H7NO-H+	e.g. Benzamide	2.00
124.05	C6H5NO2-H+	Nitrobenzene	2.00
136.04	C7H5NO2-H+	e.g. 2-Furoylacetonitrile	2.00

Table S3: Polycyclic aromatic compounds included in the SP-HR-ToF-AMS HR-PAH analysis. Analysis was based on the grouping by Herring et al. (2015) and adapted for residential wood combustion exhaust with an addition of polycyclic aromatic compounds typically released from RWC (Avagyan et al., 2016; Bertrand et al., 2018; Bruns et al., 2015; Czech et al., 2018; Miersch et al., 2019).

Unsubstituted PAHs (UnSubPAH)	Oxygenated PAHs (OPAH)	Methylated PAHs (MPAH)	Nitrogen-substituted PAHs (NPAH)	Amino PAHs (APAH)
C10H8	C9H8O	C11H10	C10H7NO2	C16H11N
C12H8	C11H8O	C12H12	C12H9NO2	C18H13NO
C12H10	**C11H8O2***	C13H12	C13H9NO2	C20H13N
C13H10	C10H6O2	C14H12	C14H9NO2	C21H13N
C14H8	C12H8O	C15H12	C16H9NO2	
C14H10	C13H8O	C15H14	C13H8N2O4	
C15H10	C13H10O	C16H14	C18H11NO2	
C16H10	**C12H6O3***	C17H16		
C17H12	C12H6O2	**C18H14***		
C18H10	C12H8O2	C18H18		
C18H12	**C12H8O3***	C19H14		
C20H10	C14H10O	C20H16		
C20H12	C13H8O2	C21H16		
C22H12	C15H8O			
C22H14	C14H8O2			
C24H12*	**C15H8O2***			
	C16H8O2			
	C16H10O*			
	C17H10O*			
	C19H10O			
	C18H10O2			

*** added for RWC**

Section S2 – OH exposure and external OH reactivity of RWC exhaust

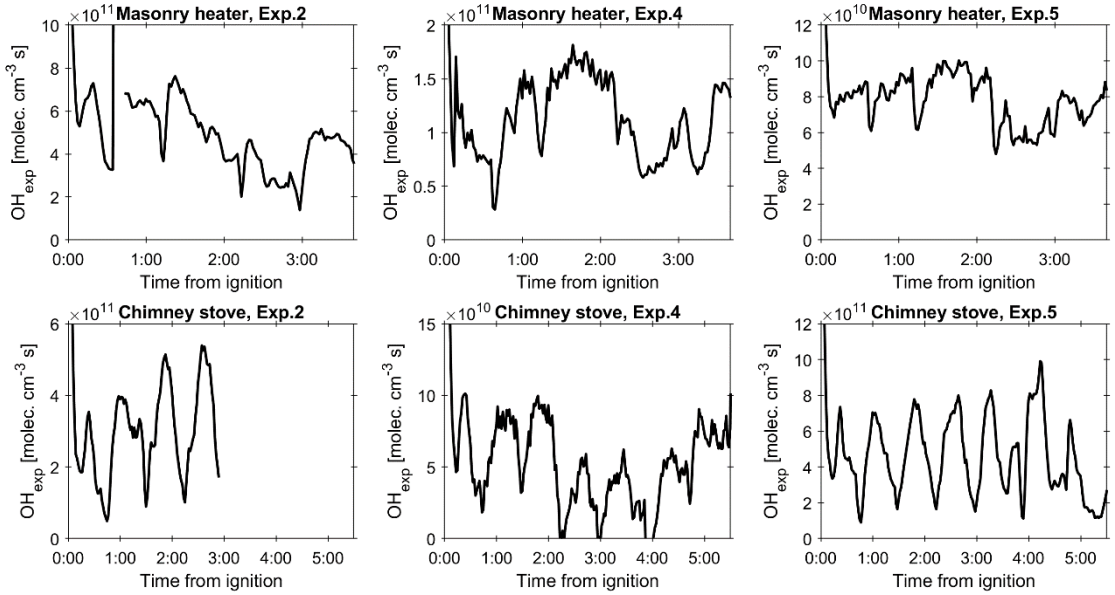

Figure S1: OH exposure during photochemical aging experiments based on the butanol-d9 decay in the PEAR OFR.

External OH reactivity ($OHR_{ext} = \Sigma\, k_i * c_i$; Li et al., 2015) was calculated from the compounds measured by FTIR from the primary exhaust, using their reaction rate constants with OH (k_i; Table S1) and dilution corrected concentrations (c_i) upstream the PEAR OFR. In addition, the butanol-d9, which was used as a marker to determine the OH-exposure, caused an additional OHR_{ext} of 9 s^{-1} (5-7 % of total) for masonry heater experiments, 7 s^{-1} (2 %) for chimney stove experiments 2 and 4 (2 %), and 17 s^{-1} in chimney stove experiment 5 (1 % of total).

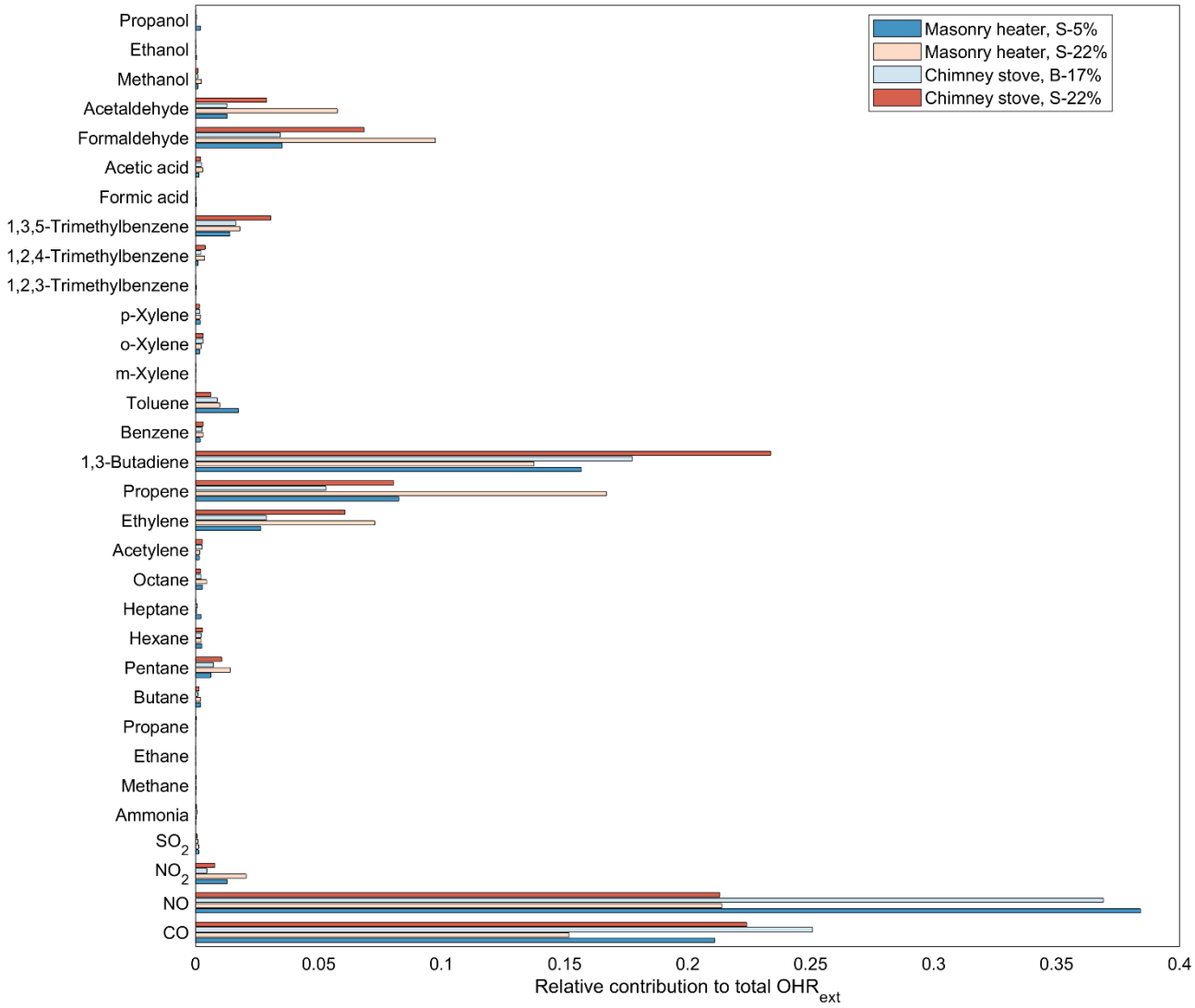

Figure S2: Average relative contributions of the gaseous compounds measured by FTIR to the external OH reactivity of primary RWC exhaust. Note that only the compounds in the exhaust itself are included, and the additional OHRext by butanol-d9 is not considered here.

Section S3 – Primary emission

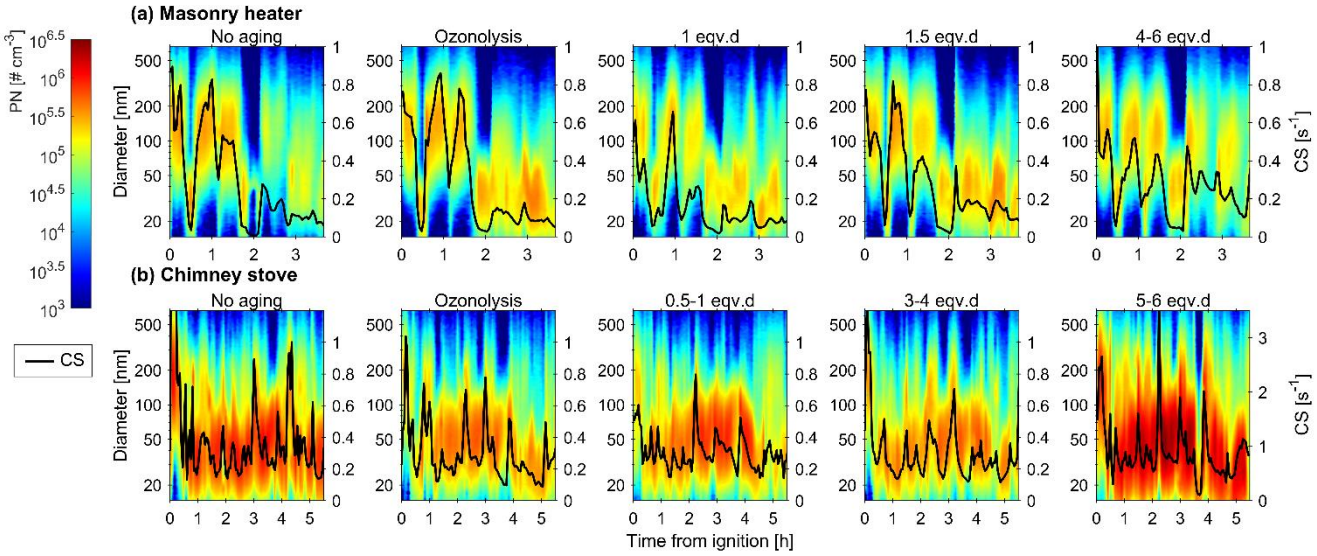

Figure S3: Size distributions of diluted primary aerosol entering the PEAR OFR reactor as a function of time, and condensation sinks (CS) in the PEAR OFR based on average size distributions measured with SMPS before and after the PEAR OFR.

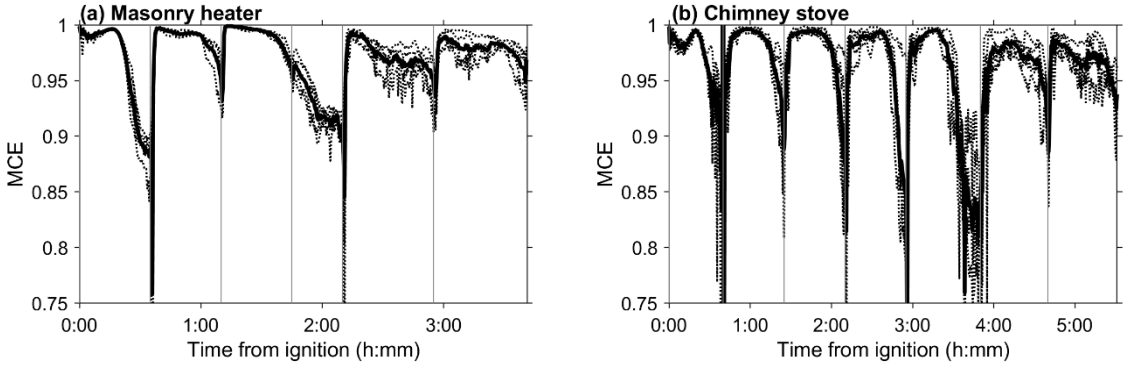

Figure S4: Modified combustion efficiency (MCE = ΔCO_2 / (ΔCO_2 + ΔCO)) during the experiments. Averages of the experiments (n=5) are shown with the solid lines and distinct experiments are shown with the dotted lines.

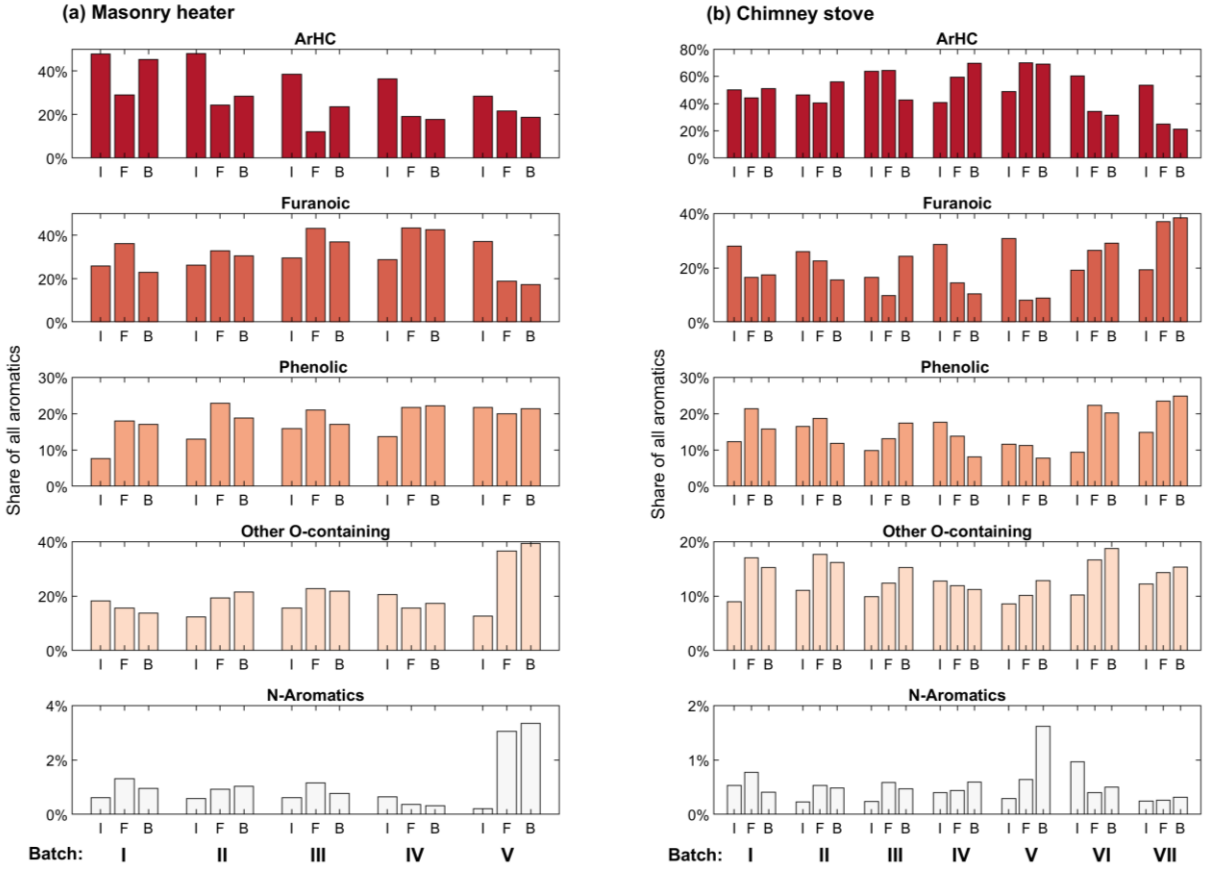

Figure S5: Average shares of the aromatic compound groups measured by PTR-ToF-MS from unaged aerosol, in relation to the total aromatic concentration (ppm:ppm) during different combustion phases (I = ignition, F = flaming, B = burnout) for each batch.

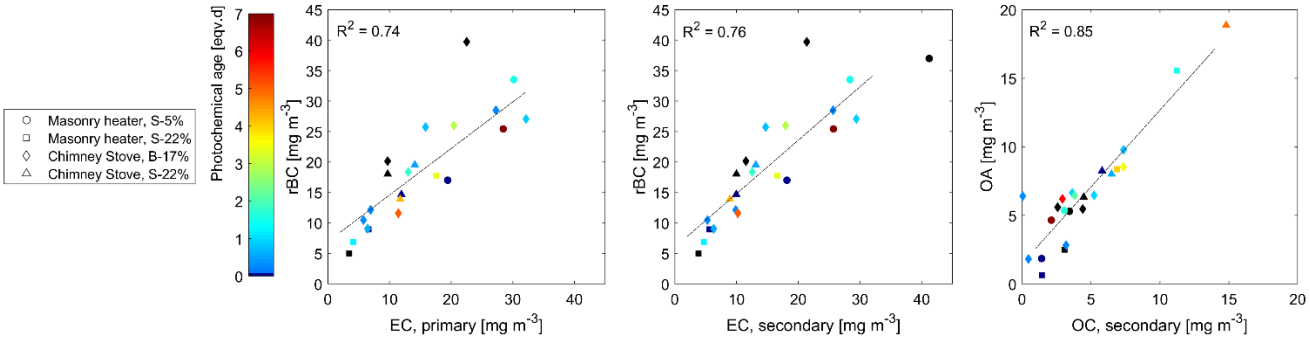

Figure S6: Correlations between variables measured by SP-HR-ToF-AMS after the PEAR OFR and by thermal-optical analyses, respectively: (a) refractory black carbon (rBC) and elemental carbon (EC) before the PEAR OFR; (b) rBC and EC after the PEAR OFR; (c) organic aerosol (OA) and organic carbon (OC) after the PEAR OFR.

Table S4: Average (± standard deviation) concentrations of gaseous emissions in the primary flue gas measured by FTIR for each experiment type (five experiments each). No O_2 reduction. Concentrations as in dry flue gas, excluding H_2O.

		Masonry heater		Chimney stove		p* Masonry heater; S-5% v. S-22%	p* Chimney stove; B-17% v. S-22%	p** S-22%; Masonry heater v. Chimney stove
Compound	unit	S-5%	S-22%	B-17%	S-22%			
Water vapor	vol-%	4.5 ± 0.3	4.1 ± 0.4	7.2 ± 0.4	6.4 ± 0.5	<0.01	<0.01	<0.01
Carbon dioxide	vol-%	4.6 ± 0.1	3.26 ± 0.08	6.2 ± 0.3	5.9 ± 0.4	<0.01	0.05	<0.01
Carbon monoxide	ppm	638 ± 26.5	735 ± 129	1680 ± 249	1880 ± 144	0.24	0.28	<0.01
Nitrogen monoxide	ppm	25.6 ± 1.8	21.4 ± 2.6	45.9 ± 2.9	31.6 ± 3.7	<0.01	<0.01	<0.01
Nitrogen dioxide	ppm	1.0 ± 0.4	2.7 ± 1.1	1.3 ± 0.7	2.6 ± 1.6	0.03	0.08	0.98
Sulfur dioxide	ppm	0.5 ± 0.3	0.6 ± 0.3	1.4 ± 0.3	0.9 ± 0.1	0.05	<0.01	0.1
Ammonia	ppm	1 ± 0.3	1.9 ± 0.3	6.2 ± 0.4	5.1 ± 0.5	<0.01	0.01	<0.01
Methane	mgC m^{-3}	10.5 ± 0.5	23.6 ± 5.6	28.7 ± 4.5	46.3 ± 4.4	<0.01	0.01	<0.01
Non-methane OGC	mgC m^{-3}	42.6 ± 9.2	101 ± 24.6	89.4 ± 11.3	148.3 ± 23	0.01	<0.01	0.05
Alkanes	mgC m^{-3}	9.7 ± 2.6	23.8 ± 6.6	16.9 ± 3	29.5 ± 6.7	<0.01	0.01	0.31
Unsaturated	mgC m^{-3}	12.8 ± 2.9	33.1 ± 8.1	30.8 ± 4.7	54.2 ± 5.4	<0.01	<0.01	<0.01
Aromatics	mgC m^{-3}	14.2 ± 3.5	20.7 ± 2.6	27.9 ± 4.9	36.0 ± 3.4	0.02	0.02	<0.01
Oxygenated	mgC m^{-3}	5.6 ± 1.2	21.9 ± 8.1	13.3 ± 0.6	27.1 ± 8.9	0.01	0.04	0.51

* paired Student's t-test; comparison of averages of the consecutive experiments; ** unpaired Student's t-test of independent experiments

Section S4 – Conditions in the PEAR OFR

S4.1. Photochemical aging conditions

OH exposure during photochemical aging was measured directly from the decay of externally added butanol-d9 (Barmet et al., 2012). Timeseries for the OH exposures during each experiment are shown in Figure S1. The relevance of other reaction pathways in the PEAR OFR, including photolysis as well as exposure to ozone, excited singlet oxygen ($O(^1D)$), and triplet atomic oxygen ($O(^3P)$), was estimated based on the estimation equations by Peng et al. (2016) (Table S5). The conditions in the PEAR OFR were assessed utilising the measured OH exposure (OH_{exp}), initial O_3 input concentration ($O_{3,\ init}$), residence time in the PEAR OFR (RT; 139 s), and water mixing ratio (H_2O; 0.015 for 45 % relative humidity). Average exposures during each experiment are shown in Table S6 and their relevance towards ambient atmospheric conditions are displayed in Figure S8.

As an example of the relevance of the different reaction pathways towards OGC fate, their importance was assessed for two important SOA precursors common for RWC: benzene and toluene (Fig. S10). The ratio of degradation by photolysis (D_{flux}) and reactions with alternative oxidants (D_X) to the degradation by OH reactions were calculated with Eq. (S1-S2), which show the inverse relationship between the importance of the pathway and the ratio of the photoabsorption cross section (σ_{abs}) or reaction rate of the compound with the considered radical ($k[X]_{OGC}$) to its reaction rate with OH ($k[OH]_{OGC}$).

$$D_{flux} = \frac{flux_{exp}}{[OH]_{exp}} * \frac{\sigma_{abs,\mathrm{OGC}}}{k[OH]_{\mathrm{OGC}}} \quad \text{(S1)}$$

$$D_x = \frac{[X]_{exp}}{[OH]_{exp}} * \frac{k[X]_{\mathrm{OGC}}}{k[OH]_{\mathrm{OGC}}} \quad \text{(S2)}$$

The absorption cross sections and reactivities used for the exemplary pathway estimations for toluene and benzene are listed in Table S7. The total degradation in relation to degradation by OH was calculated with Eq. (S3) by considering reactions with OH, O_3, and $O(^3P)$ and photolysis.

$$D_{total} = 1 + D_{flux} + D_{O3} + D_{O(3P)} \quad \text{(S3)}$$

Table S5: Estimation equations used for determination of photon flux (F_{254nm}), $O(^3P)$, $O(^1D)$, and O_3 exposures, based on Peng et al. (2016).

Reactant	Exposure estimation equation	eq.no
Photon flux	$flux_{254nm,exp} = 10^{\left(1.0238+\sqrt{(-1.0238)^2-4*0.060786*c}\right)/2*0.060786}$ where $c = -\left[log_{10}\left(OH_{exp}*\frac{180}{RT}\right) - \left\{15.514 + 0.79292*log_{10}(H_2O) + 0.023076*log_{10}(H_2O)^2 - log_{10}\left(1+e^{\frac{-0.42602-log_{10}\left(\frac{O_{3,init}}{OHR_{ext}}\right)}{0.39479}}\right)\right\}\right]$	(S4)
$O(^1D)$	$\log_{10}(O(^1D)_{exp}) = 3.7371 + 0.1608*\log_{10}\left(-\log_{10} d^{\frac{180}{RT}}\right) - 1.1344*\log_{10} H_2O + 0.59179*\log_{10} O_3,init - 0.17019*\log_{10}\left(-\log_{10} d^{\frac{180}{RT}}\right)*\log_{10} H_2O - 0.37983*\log_{10}\left(-\log_{10} d^{\frac{180}{RT}}\right)^2 + 0.099941*\log_{10} OHR_{ext}$	(S5)
$O(^3P)$	$\log_{10}(O(^3P)_{exp}) = 7.6621 + 0.16135*\log_{10}\left(-\log_{10} d^{\frac{180}{RT}}\right) - 1.1342 * \log_{10} H_2O + 0.59182 * \log_{10} O_{3,init} - 0.17007*\log_{10}(-\log_{10} d^{\frac{180}{RT}}) * \log_{1o} H_2O - 0.3797*(\log_{10}(-\log_{10} d^{\frac{180}{RT}}))^2 + 0.099902*\log_{10}(OHR_{ext})$	(S6)
O_3	$\log_{10}(O_{3,exp}) = 15.559 + \log_{10} O_{3,init} + 0.42073*\log_e(d^{180/RT})$	(S7)
for Eq. S5–S7:	$d = \left(10^{-10}\right)^{\log_{10}(OH_{exp}/RT*180) - 13.322 + 0.22101*\left(\frac{OHR_{ext}}{O_{3,init}}\right)^{0.43529}}{}^{RT/180}$	(S8)

Table S6: Average radical exposures in the PEAR OFR during photochemical aging experiments.

	Exp.	O_3 input [ppm]	photon flux [photons cm^{-2}]	Fuel	OH_{exp} [s cm^{-3}]	$O(^1D)_{exp}$ [s cm^{-3}]	$O(^3P)_{exp}$ [s cm^{-3}]	$O_{3\ exp}$ [s cm^{-3}]
Masonry heater	2	2.3	8.6E+15	S-5%	5.8E+11	1.3E+06	1.1E+10	2.3E+15
				S-22%	3.5E+11	1.2E+06	9.9E+09	2.9E+15
	4	2.2	2.8E+15	S-5%	1.5E+11	5.2E+05	4.4E+09	5.2E+15
				S-22%	1.3E+11	8.6E+05	7.2E+09	4.0E+15
	5	1.8	1.4E+15	S-5%	8.1E+10	3.0E+05	2.5E+09	4.9E+15
				S-22%	6.3E+10	3.9E+05	3.3E+09	4.6E+15
Chimney stove	2	4.3	5.8E+15	B-17%	3.1E+11	1.6E+06	1.3E+10	6.5E+15
				S-22%*	not meas.	not meas.	not meas.	not meas.
	4	3.6	1.1E+15	B-17%	5.4E+10	3.0E+05	2.6E+09	1.1E+16
				S-22%	6.1E+10	4.1E+05	3.4E+09	1.0E+16
	5	11	1.1E+16	B-17%	5.0E+11	4.4E+06	3.7E+10	8.8E+15
				S-22%	5.0E+11	5.2E+06	4.4E+10	6.7E+15

*Direct OH exposure measurements not available for Chimney stove Exp.2 S-22%; approximately similar as in Exp.2 B-17%.

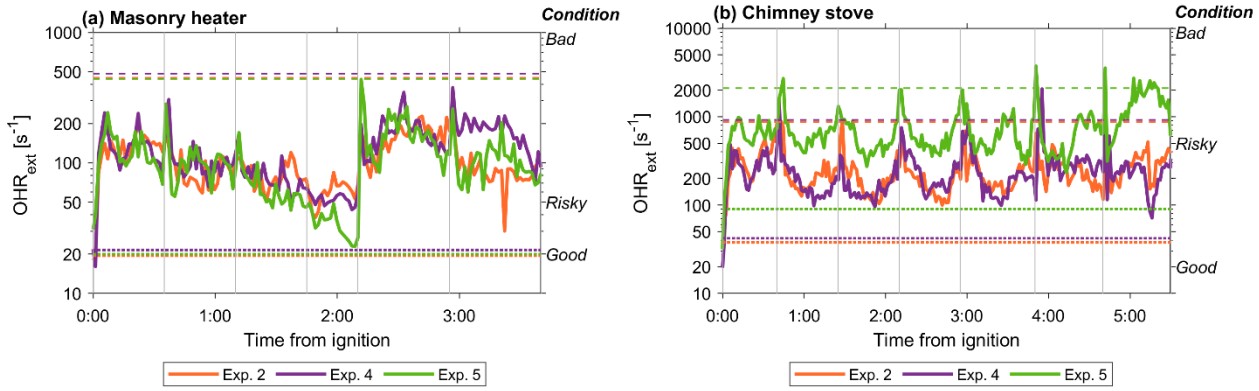

Figure S7: External OH reactivity in the PEAR OFR during photochemical aging experiments, including OHR_{ext} by butanol-d9 and the compounds measured by FTIR. Risk levels for OHR_{ext} determined by Peng and Jimenez (2017) are marked with dotted (good/risky: $\frac{Flux_{254nm}\ exposure}{OH\ exposure}$ > 4 × 10^5 cm s^{-1}) and dashed (risky/bad: $\frac{Flux_{254nm}\ exposure}{OH\ exposure}$ >10^7 cm s^{-1}) lines for each experiment.

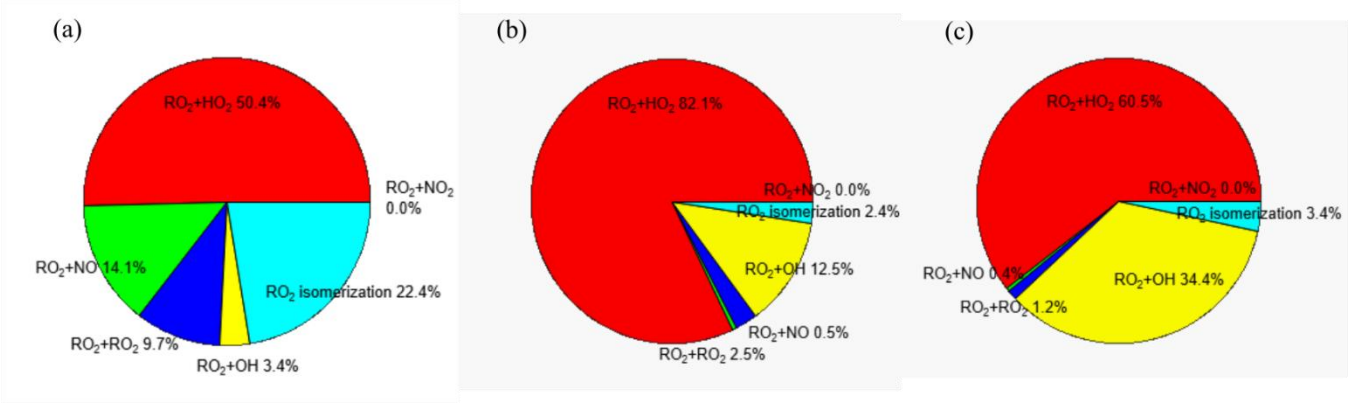

Figure S8: Rough estimation of the relative shares of RO_2 fates in (a) ambient air at OHR_{ext} = 10, and (b-c) in the PEAR OFR during the first minute of aging, during which majority of the volatile organic compounds are expected to have reacted. Shown for two experiments with different aging conditions: (b) high OH exposure (masonry heater Exp. 2) and (c) high OHR_{ext} (chimney stove Exp. 5). Based on the RO_2 Fate Estimator by Peng et al. (2019).

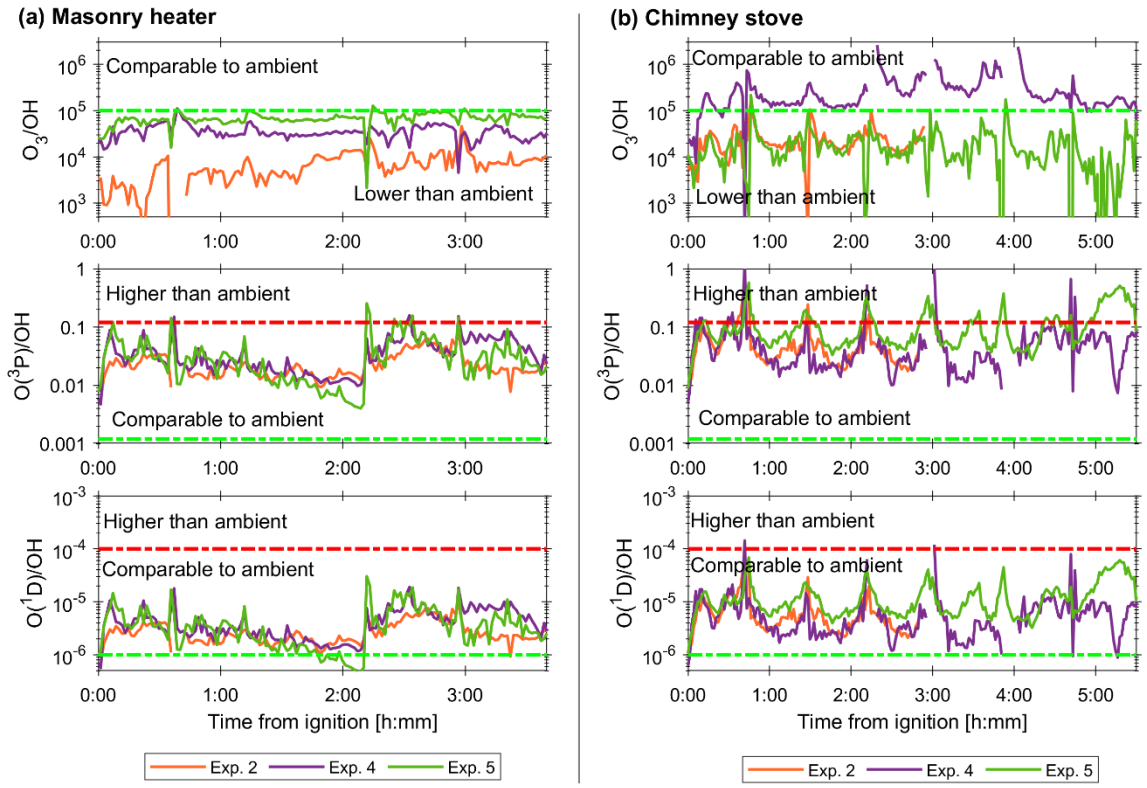

Figure S9: Ratios of alternative reaction pathways to the OH exposure and their relevance towards ambient conditions. Ambient ratios as in Peng et al. (2016).

Table S7: Absorption cross sections (σ_{abs}, cm^2 $molecule^{-1}$) and reaction rates (cm^3 $molec.^{-1}$ s) of some of the major volatile organic compounds from RWC towards oxidants in the PEAR OFR.

	Benzene	Toluene	Phenol	Furan	Acetic acid	Acetaldehyde	Isoprene	References
$\sigma_{abs,\ 254nm}$	3.0E-19	2.3E-19	1.6E-18	7.1E-19*	4.8E-21	1.5e-20	5.3E-20	Keller-Rudek et al. (2015); * at 225nm
k[OH]	1.8E-12 [A]	6.16E-12 [A]	1.00E-11[B]	4.04E-11[A]	8.00E-13[C]	1.62E-11[A]	1.00E-10[A]	A: (Atkinson, 1986), B: (Baulch et al., 1992); C: (Atkinson. et al., 2001)
k[O_3]	1.72E-22[A]	3.90E-22[A]		2.42E-18[B]		3.40E-20[c]	1.29E-17[D]	A: (Toby et al., 1985), B: (Atkinson et al., 1983) C: (Stedman and Niki, 1973), D: (Grosjean and Grosjean, 1996)
k[$O(^3P)$]	1.99E-14[A]	7.63E-14[A]	1.56E-13[B]		1.73E-15[C]	4.58E-13[B]	3.50E-11	A: (Cvetanović, 1987), B: (Baulch et al., 1994), C: (Herron, 1988), (Paulson et al., 1995)

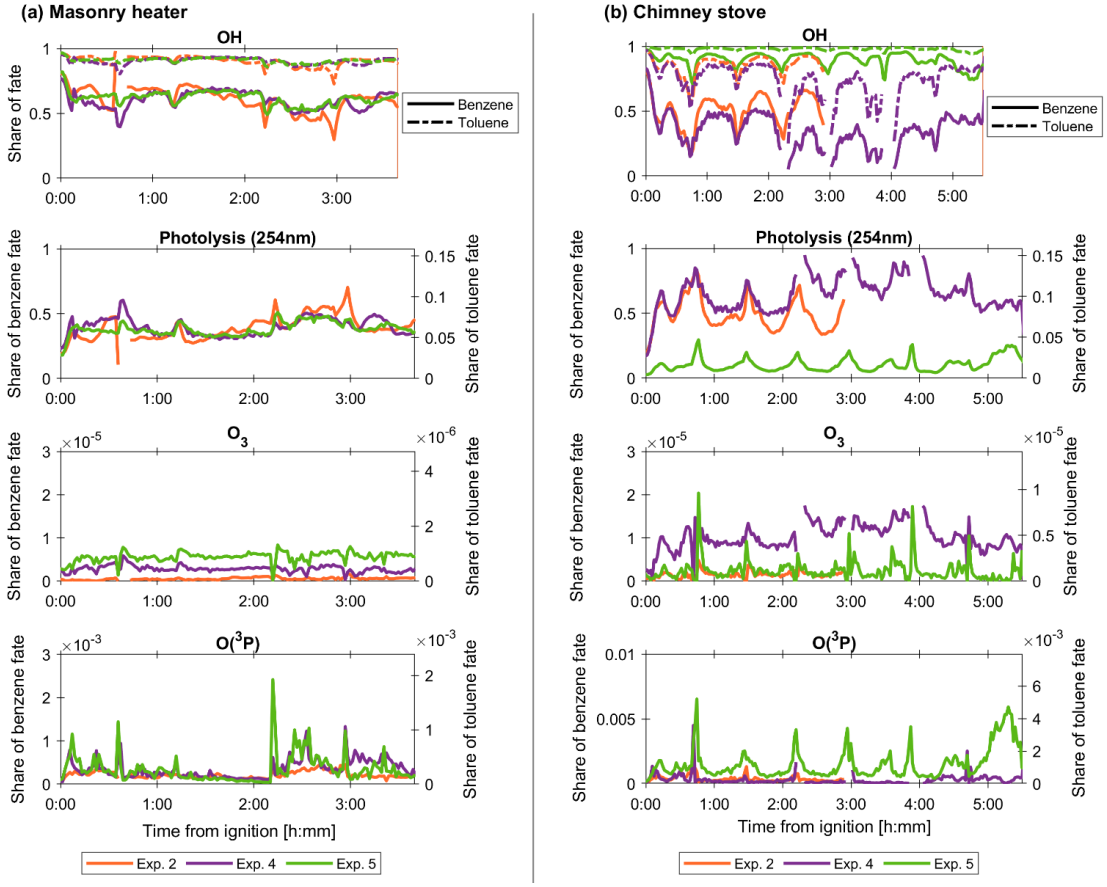

Figure S10: Share of the considered pathways to the degradation of benzene and toluene in the PEAR OFR during the photochemical aging experiments.

S4.2 Fate of low-volatility organic compounds in the PEAR OFR

Estimations of the LVOC fates in the PEAR OFR were done based on Palm et al. (2016). Three possible pathways for LVOC depletion in the PEAR OFR were considered: condensation onto particles, reactions with OH, and condensation onto walls of the PEAR OFR. The rest exit the PEAR OFR in the gas-phase after which they are expected to condense on the walls of sampling lines.

The LVOC lifetime due to aerosol losses (τ_{aer}) was calculated using Eq. (S9):

$$\tau_{aer} = \frac{1}{CS} \quad \text{(S9)}$$

where condensation sink (CS, s^{-1} ; Fig. S3) was calculated according to Lehtinen et al. (2003), using an average of the particle size distributions before and after the PEAR OFR. The diffusion coefficient in use (D; 7×10^{-6} m^2 s^{-1}) was chosen as representative for oxidised, ~200 g mol^{-1} molecules (Tang et al., 2015).

LVOC lifetime due to wall losses (τ_{wall}) was calculated with Eq. (S10):

$$\tau_{wall} = \left(\frac{A}{V} * \frac{2}{\pi}\sqrt{k_e D}\right)^{-1} \quad \text{(S10)}$$

τ_{wall} depends on the area-to-wall ratio ($\frac{A}{V}$), which in the PEAR OFR is 2.28 m^2:0.139 m^3 = 16.4 m^{-1}. The applied eddy diffusion coefficient, k_e, was 0.0036 s^{-1}, similarly to Palm et al. (2016). τ_{wall} was constant (603 s) for all of the PEAR OFR experiments.

Lifetime for LVOCs due to reactions with OH radicals was calculated with Eq. (S11):

$$\tau_{OH} = \frac{5}{k_{OH} * [OH]} \quad \text{(S11)}$$

based on the estimations that LVOCs as a total have an OH reaction rate (k_{OH}) of 1×10^{-11} cm^3 $molec.^{-1}$ s^{-1} and that it takes five such reactions for LVOC fragmentation into higher-volatility compounds.

The resulting total lifetime was calculated with Eq. (S12):

$$\tau_{total} = \left(\frac{1}{\tau_{aer}} + \frac{1}{\tau_{wall}} + \frac{1}{\tau_{OH}}\right)^{-1} \quad \text{(S12)}$$

from which the fraction of each pathway (F_x, where footnote denotes the degradation pathway: aerosol, wall, or OH) to the total loss was derived with Eq. (S13).

$$F_x = (1 - F_{exit}) * \frac{\tau_x{}^{-1}}{\tau_{total}{}^{-1}} \quad \text{(S13)}$$

The fraction of LVOCs exiting the PEAR OFR in gas-phase (F_{exit}) was by Eq. (S14):

$$F_{exit} = e^{-\frac{RT}{\tau_{total}{}^{-1}}} \quad \text{(S14)}$$

with the residence time (RT) being 139s for the 60lpm flow rate.

F_{aer} was by far the most important fate of the LVOCs in the PEAR OFR throughout the experiments (Fig. S11). The amount of LVOCs estimated to exit the PEAR OFR as gas-phase LVOCs exceeded 0.1 % only during the middle burnout phase of the masonry heater combustion because of the low particle number concentrations during the char burning phase between the change from dry spruce to moist spruce combustion, which generated a low condensation sink into the PEAR OFR.

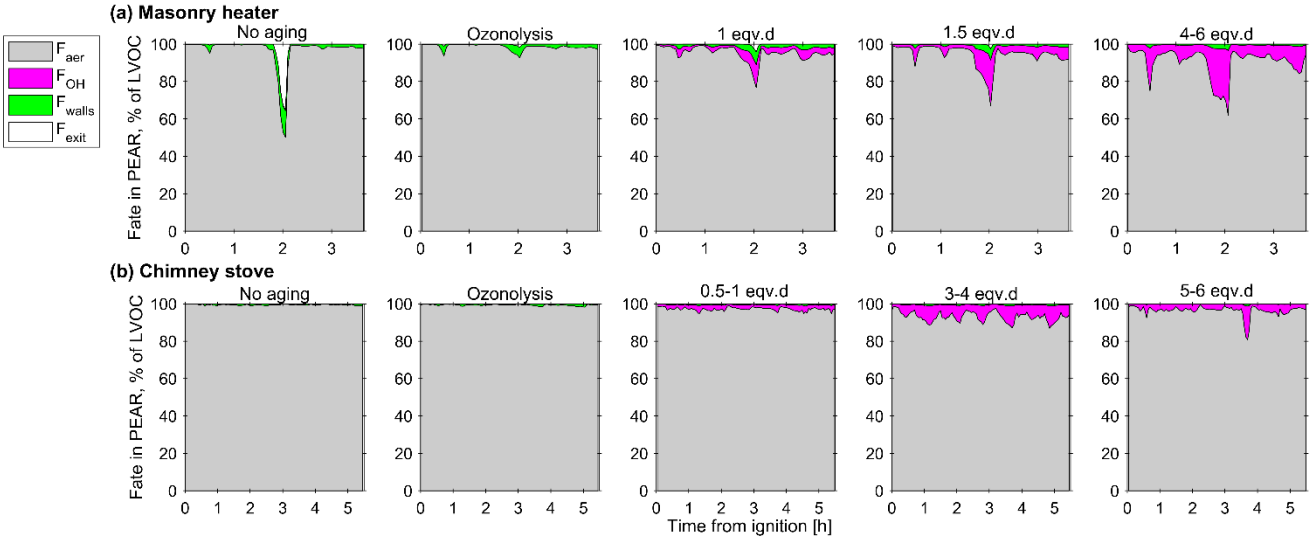

Figure S11: Estimated fates of the low-volatility organic compounds in the PEAR OFR during the experiments with portions of the LVOCs condensing onto particles (F_{aer}) and walls (F_{walls}) and lost in reactions with OH (F_{OH}). The remainder of the LVOCs (F_{exit}) exit the PEAR OFR.

Section S5 – Transformation of the particulate phase

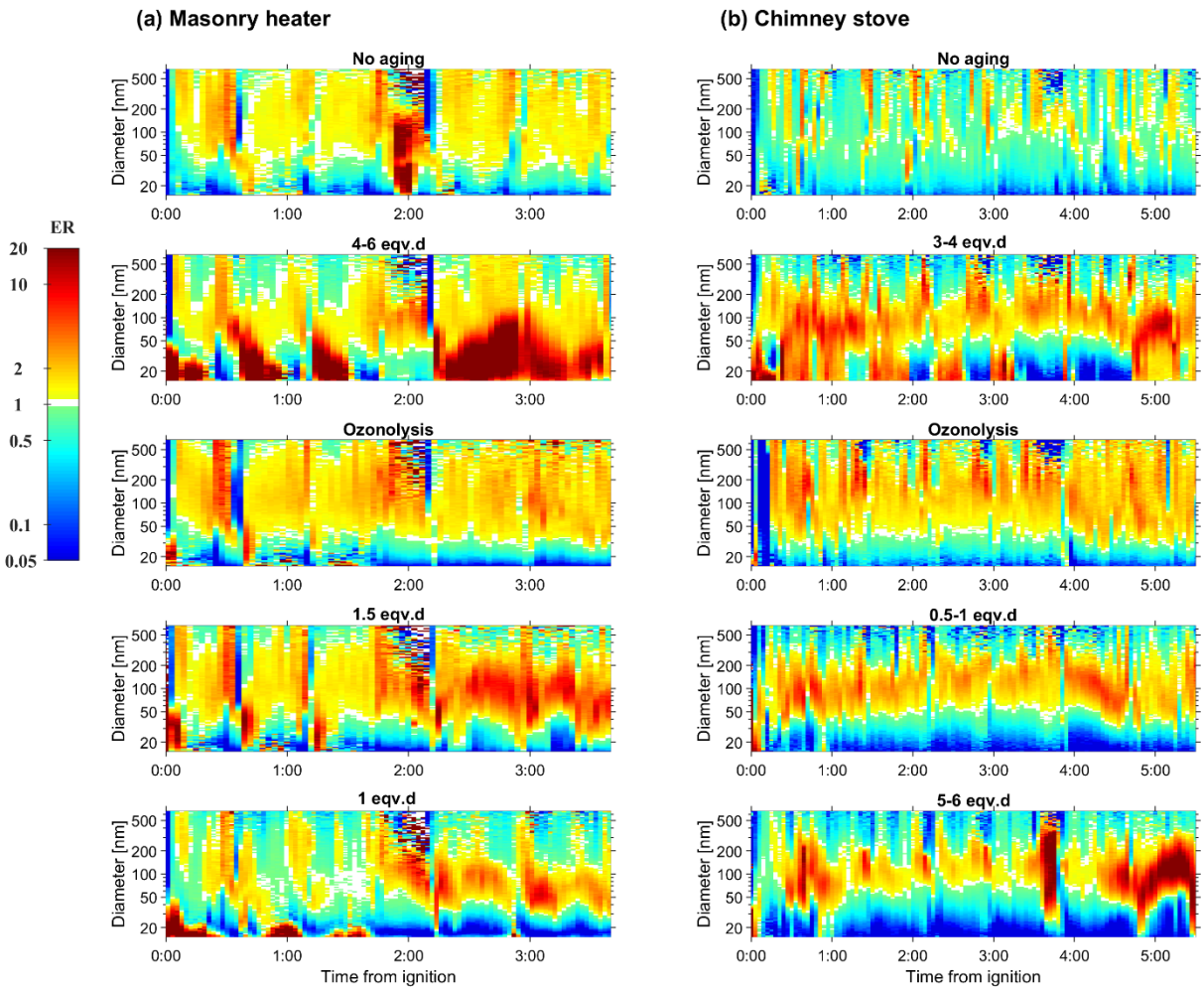

Figure S12: Particle number enhancement ratios (ER; ratio of secondary to primary concentration) in each experiment, based on the SMPS measurements before and after the PEAR OFR.

Table S8: Average chemical composition of the particulate matter (normalised to dry, 13 % O_2 flue gas conditions) measured by SP-HR-ToF-AMS.

	Exp.	Fuel	Exposure [eqv.d]	O:C	H:C	OS_C	OM:OC	rBC [mg m^{-3}]	OA [mg m^{-3}]	PAH [µg m^{-3}]	NO_3 [mg m^{-3}]	SO_4 [mg m^{-3}]	NH_4 [mg m^{-3}]	Chl [mg m^{-3}]
Masonry heater	1	S-5%		0.55	1.51	-0.18	1.86	28.89	3.10	98	0.16	0.17	0.00	0.17
		S-22%		0.82	1.33	0.15	2.20	21.77	1.57	27	0.11	0.13	0.00	0.12
	2	S-5%	6.72	1.45	1.06	0.92	3.02	42.83	7.63	16	1.92	0.80	0.79	0.02
		S-22%	4.02	1.30	1.12	0.64	2.83	48.03	24.98	80	1.50	1.08	0.96	0.03
	3	S-5%	O_3	0.69	1.38	0.00	2.03	68.54	9.64	246	1.42	0.21	0.03	0.13
		S-22%	O_3	0.81	1.28	0.15	2.19	12.15	6.61	180	0.84	0.25	0.03	0.06
	4	S-5%	0.94	0.90	1.31	0.22	2.31	59.40	9.58	105	1.27	0.44	0.16	0.04
		S-22%	0.73	0.84	1.33	0.17	2.23	17.70	44.11	485	1.00	0.38	0.49	0.04
	5	S-5%	1.71	0.76	1.36	0.07	2.13	47.08	13.69	241	1.36	0.27	0.16	0.05
		S-22%	1.46	0.78	1.34	0.11	2.16	24.47	24.54	455	1.20	0.37	0.24	0.03
Chimney stove	1	B-17%		0.86	1.25	0.22	2.26	23.03	3.86	65	0.34	1.08	0.00	0.28
		S-22%		1.47	0.91	0.41	2.32	27.97	4.02	80	0.21	1.13	0.00	0.31
	2	B-17%	3.61	1.25	1.14	0.63	2.76	21.60	8.78	23	5.07	1.66	1.38	0.02
		S-22%	~4	1.47	1.19	0.90	2.80	19.70	10.39	26	4.05	1.33	0.96	0.02
	3	B-17%	O_3	1.01	1.15	0.41	2.44	26.24	8.33	114	3.32	1.82	0.22	0.12
		S-22%	O_3	0.82	1.30	0.16	2.20	24.89	10.34	271	2.41	1.12	0.16	0.13
	4	B-17%	0.62	1.09	1.17	0.47	2.55	20.93	9.95	52	10.90	2.93	1.88	0.08
		S-22%	0.70	1.04	1.23	0.05	2.37	27.91	11.46	215	6.40	1.89	1.02	0.08
	5	B-17%	5.78	1.36	1.11	0.80	2.91	21.81	9.45	22	7.34	2.68	1.66	0.02
		S-22%	5.83	0.87	1.32	0.10	2.74	19.63	32.71	158	4.63	1.26	1.31	0.03

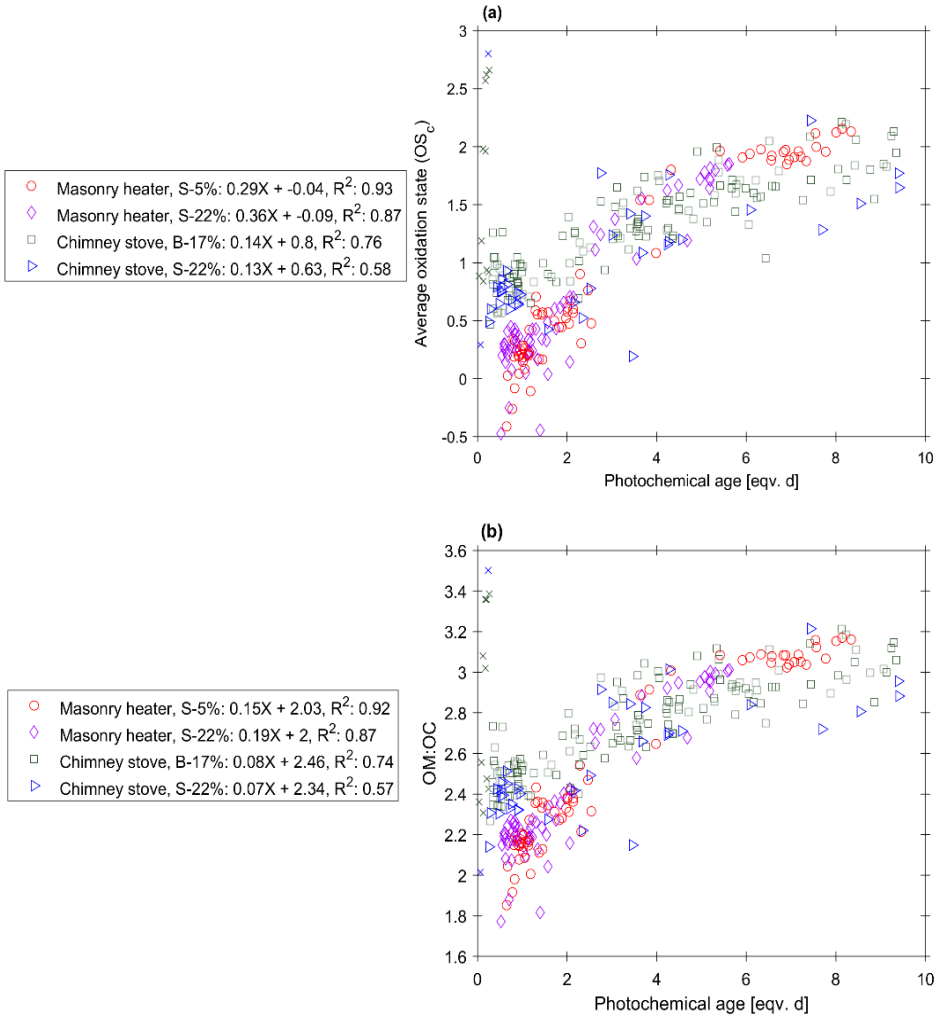

Figure S13: Relationship between photochemical age and (a) oxidation state and (b) OM:OC ratio measured by SP-HR-ToF-AMS during the photochemical aging experiments. Coefficients of determination (R^2) were calculated for the photochemical exposure range of 0.25-10 eqv.d. Values outside this age range (crossed over) were not considered.

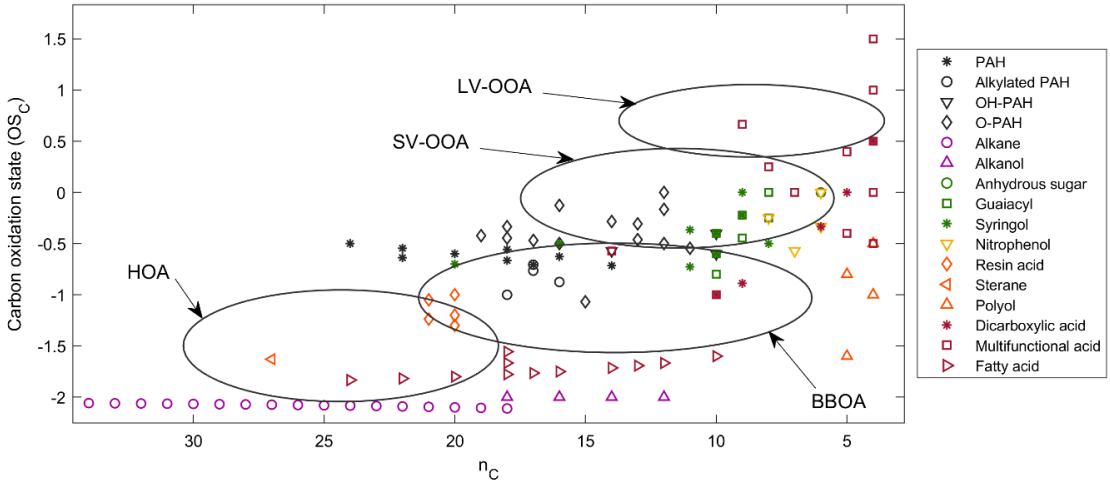

Figure S14: Compounds analysed by IDTD-GC-ToFMS displayed in the OS_C-n_C space. Approximate areas for ambient organic aerosol classes are presented to give approximate references for average ambient hydrocarbon-like OA (HOA), primary biomass burning OA (BBOA), semi-volatile oxidised OA (SV-OOA) and low-volatility oxidised OA (LV-OOA), as identified by Kroll et al. (2011)

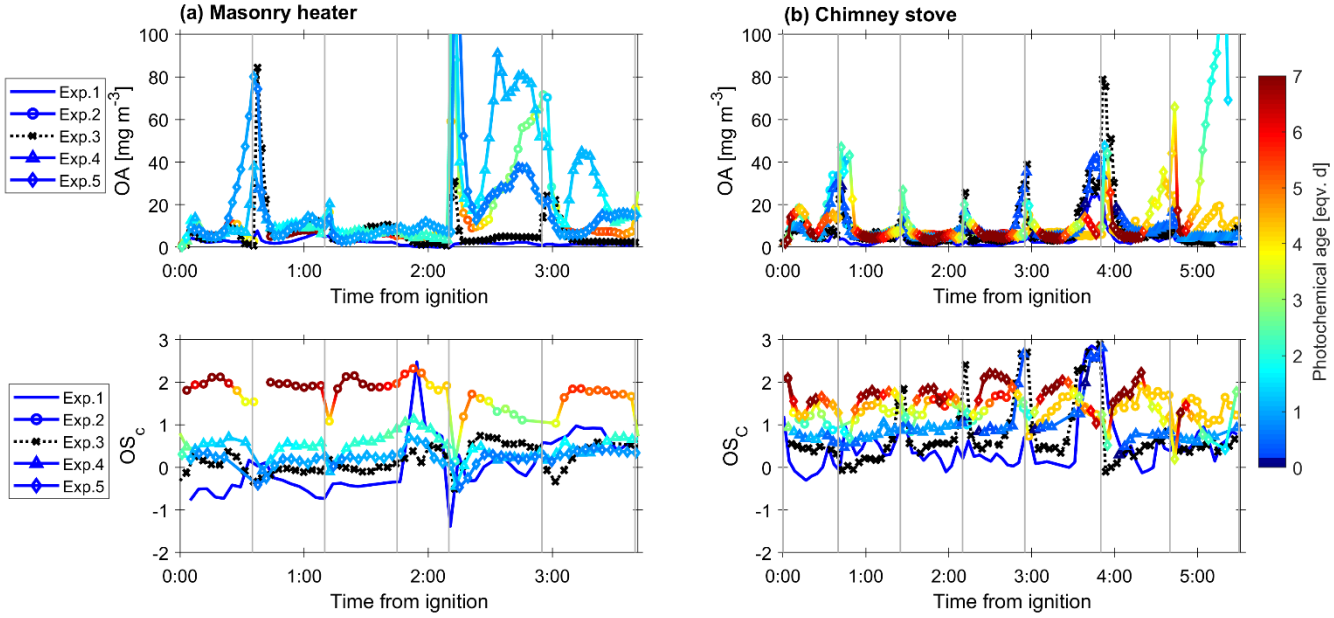

Figure S15: Concentrations and average carbon oxidation states (OS_C) of particulate OA from (a) masonry heater and (b) chimney stove measured by SP-HR-ToF-AMS downstream the PEAR OFR, normalised to dry, 13 % O_2 flue gas conditions. Black dotted lines indicate ozonolysis experiments.

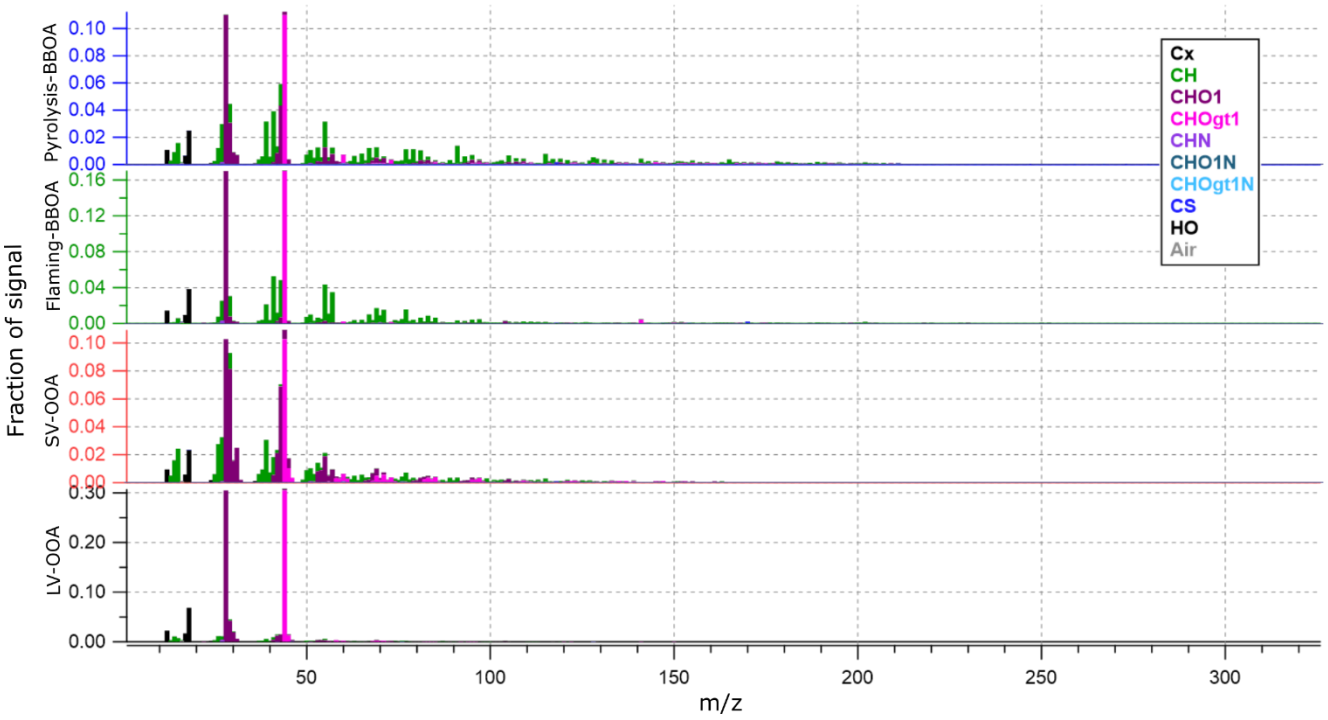

Figure S16: Spectra of the four factors identified from the SP-HR-ToF-AMS OA spectra by positive matrix factorisation analysis.

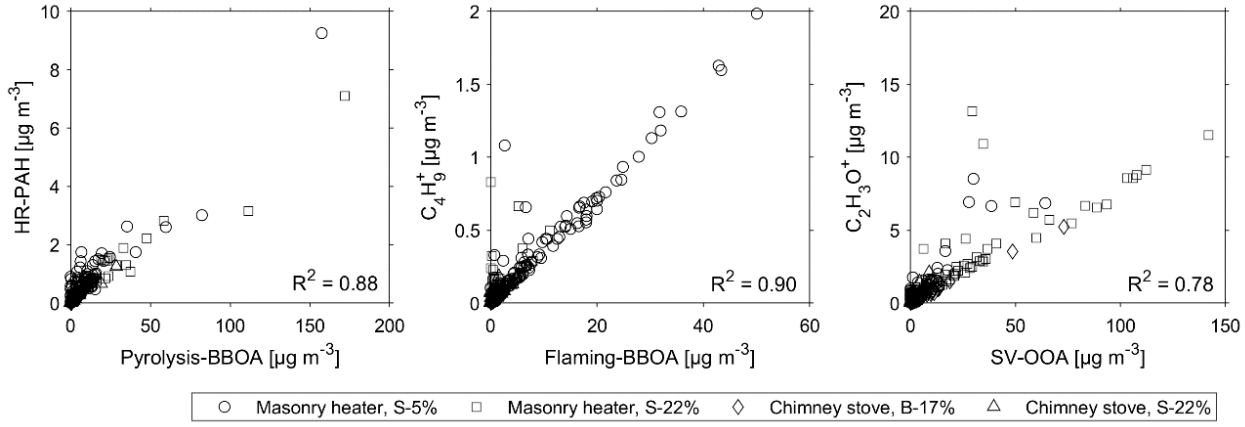

Figure S17: Correlations between (a) pyrolysis-BBOA and HR-PAH, (b) flaming-BBOA and $C_4H_9^+$, and (c) SV-OOA to $C_2H_3O^+$, measured by SP-HR-ToF-AMS from the diluted exhaust downstream the PEAR OFR.

S5.1 In-situ derivatisation and thermal desorption - gas-chromatography - time-of-flight mass spectrometry

In-situ derivatisation and thermal desorption - gas-chromatography - time-of-flight mass spectrometry (IDTD-GC-ToFMS, (Orasche et al., 2011) was utilised in analysis of semi volatile organic target analytes in particulate phase. Subsamples were taken from the collected quartz fibre filters and prepared in GC-liners for the analyses. 10 µl Methyl-trimethylsilyl-trifluoroacetamid (MSTFA, Macherey-Nagel, Germany) was added automatically in each liner by the sampling robot (PAL Focus, Atas GL, Netherlands) before samples were placed into a direct thermal desorption unit (Linex and Optic 3, Atas GL, Netherlands). The samples were spiked with mixtures of isotope labelled internal standards and calibration standards for the purpose of calibration and quantification of the polar (Table S9) and non-polar (Table S10) compounds.

MSTFA was continuously added to the helium carrier gas on a 4 ml min^{-1} stream, throughout the 16 minutes of thermal extraction at 300 °C. After the thermal extraction and derivatisation procedure, the pure helium flow was set back to 0.7 ml min^{-1}, with a split flow of 50 ml min^{-1}. IDTD was done at an isothermal GC temperature of 50° C in order to trap desorbed compounds at the front of the separation column before starting the GC-MS run. The column in use was an almost non-polar BPX5, 25 m, 0.22 mm ID, 0.25 µm film thicknesses (SGE, Australia), used in an Agilent 6890 gas chromatograph (Agilent, USA). Mass spectrometric detection in the range 35 to 500 m/z was carried out on a Pegasus III ToFMS (LECO, USA) using an acquisition frequency of 25 spectra per second. Evaluation of mass spectra was done with the ChromaTOF software package (LECO, USA).

Table S9: Isotopically labelled internal standards used for polar compounds in the IDTD-GC-ToFMS analyses.

Isotopically labelled internal standard mixture	Calibration standard mixture	
4-Nitrophenol d4	1-Hydroxypyrene	Glutaric acid
Adipic acid d10	2-Hydroxy-1-naphthaldehyde	Hexanedioic acid
Cholesterol d6	2-Ketoglutaric acid	Hexanoic acid
Dodecanol d25	2-Methyl-4-Nitrophenol	Isopimaric acid
Fumaric acid d2	2-Methylerythritol	Levoglucosan
Glucose 13C6	2-Naphthanol	Linoleic acid
Glycerol d8	3-Hydroglutaric acid	Maleic acid
Levoglucosan 13C6	3-Hydroxyphenanthrene	Malic acid
Palmitic acid d31	4-Hydroxyphenanthrene	Malonic acid
Vanillin 13C6	4-Nitrocatechol	Mannosan
	4-Nitrophenol	Methyl vanillate
	9-Hydroxyphenanthrene	Oleic acid
	Abietic acid	Palmitic acid
	Acetosyringone	Phthalic acid
	Adipic Acid	Salicylic acid
	Azelaic acid	Sorbit
	Butanedioic acid	Stearic acid
	Cholesterol	Syringic Acid
	Coniferaldehyde	Tartaric acid
	Ergosterol	Threitol
	Erythritol	Trimellitic acid
	Fumaric acid	Vanillic acid
	Galactosan	Vanillin

Table S10: Isotopically labelled internal standards for nonpolar compounds used in the IDTD-GC-ToFMS analyses.

Isotopically labelled internal standard mixture	Calibration standard mixture	
9,10-Anthracenedione 13C6	1(2H)-Acenaphthylenone	Benz[a]pyrene
Acenaphthene d10	1,2,4-Trimethylanthracene	Benz[e]pyrene
Acenaphthylene d8	1,2-Dimethylnaphthalene	Benzo[a]anthracene-7,12-dione
Anthracene d10	1,3,6,8-Tetramethylpyrene	Benzo[b]fluoranthene
Benz[a]anthracene d12	1,3,7-Trimethylnaphthalene	Benzo[b]fluoranthene
Benz[a]pyrene d12	1,4-Naphthoquinone	Benzo[b]naphtho[1,2-d]thiophene
Benz[e]pyrene d12	1,8-Naphthalic anhydride	Benzo[b]naphtho[2,1-d]furan
Benzo[a]anthracene-7,12-dione d10	11H-Benzo[a]fluoren-11-one	Benzo[b]naphtho[2,1-d]thiophene
Benzo[b]fluoranthene d12	11H-Benzo[b]fluoren-11-one	Benzo[b]naphtho[2,3-d]furan
Benzo[bfluoranthene d12	1-Ethylpyrene	Benzo[c]phenanthrene
Benzo[ghi]perylene d12	1-Methyl-benz[a]anthracene	Benzo[ghi]perylene
Benzo[k]fluoranthene d12	1-Methylfluorene	Benzo[k]fluoranthene
Benzo[k]fluoranthene d12	1-Methylpyrene	Benzo[k]fluoranthene
Biphenyl d10	1-Naphthaldehyde	Biphenyl
Chrysene d12	2,2'-Binaphthalene	Chrysene
Coronene d12	2,3,6,7-Tetramethylanthracene	Coronene
Dibenz[ah]anthracene d14	2,6-Dimethoxybenzoquinone	Cyclopenta(def)phenanthrenone
Dibenzothiophene d8	2-Phenylnaphthalene	Dibenz[ac]anthracene
Docosane d46	3,6-Dimethylphenanthrene	Dibenz[ah]anthracene
Eicosane d42	3-Methylfluorene	Dibenzothiophene
Fluoranthene d10	4,5-Dimethylpyrene	Fluoranthene
Fluorene d10	5,12-Naphthacenedione	Fluorene
Hexadecane d34	6-Ethylchrysene	Indeno[1,2,3-cd]pyrene
Indeno[1,2,3-cd]pyrene d12	7,12-Dimethyl-Benz[a]anthracene	Methyleicosanoate
Naphthalene d8	9,10-Anthracenedione	n-Alkanes C12-C40
Octadecane d38	9,10-Dimethylphenanthrene	Naphthalene
Perylene d12	9H-Fluoren-9-one	Naphtho[2,1,8,7-klmn]xanthene
Phenanthrene d10	9-Methylphenanthrene	Perylene
Pyrene d10	Acenaphthene	Phenanthrene
Tetracosane d50	Acenaphthonquinone	Picene
Triacontane d62	Acenaphthylene	Pyrene
	Anthracene	Retene
	Benz[a]anthracene	Xanthone

Table S11: Secondary concentrations (ng m^{-3}) of compounds measured by IDTD-GC-ToFMS. Normalised to dry, 13 % O_2 flue gas conditions. Attached as a .xlsx file

Table S12: Pearson correlation coefficients between the particulate organic aerosol constituents measured by SP-HR-ToF-AMS (PMF and HR-PAH) and IDTD-GC-TOF-MS.

		PMF factors				HR-PAH					
		Pyrolysis-BBOA	Flaming-BBOA	SV-OOA	LV-OOA	Total	Unsub-PAH	OPAH	MPAH	NPAH	APAH
PMF factors	Pyrolysis-BBOA	1.00	0.17	0.40	-0.02	**0.96**	**0.96**	**0.87**	**0.97**	**0.86**	**0.89**
	Flaming-BBOA	0.17	1.00	-0.07	-0.21	0.19	0.21	0.17	0.14	0.17	0.21
	SV-OOA	0.40	-0.07	1.00	0.35	0.48	0.44	**0.70**	0.38	**0.68**	0.57
	LV-OOA	-0.02	-0.21	0.35	1.00	-0.02	-0.04	0.09	-0.04	0.06	0.03
HR-PAH	Total	**0.96**	0.19	0.48	-0.02	1.00	**1.00**	**0.94**	**0.99**	**0.94**	**0.96**
	UnsubPAH	**0.96**	0.21	0.44	-0.04	**1.00**	1.00	**0.93**	**0.99**	**0.93**	**0.95**
	OPAH	**0.87**	0.17	**0.70**	0.09	**0.94**	**0.93**	1.00	**0.88**	**0.98**	**0.94**
	MPAH	**0.97**	0.14	0.38	-0.04	**0.99**	**0.99**	**0.88**	1.00	**0.88**	**0.92**
	NPAH	**0.86**	0.17	**0.68**	0.06	**0.94**	**0.93**	**0.98**	**0.88**	1.00	**0.97**
	APAH	**0.89**	0.21	0.57	0.03	**0.96**	**0.95**	**0.94**	**0.92**	**0.97**	1.00
IDTD-GC-ToF-MS	PAH	0.01	**0.64**	-0.22	-0.17	0.19	0.27	0.04	0.15	0.09	0.09
	OH-PAHs	0.31	-0.05	**0.88**	**0.65**	**0.75**	**0.65**	**0.92**	0.54	**0.88**	**0.87**
	Carbonyl-PAHs	0.50	-0.12	0.49	0.35	**0.69**	**0.67**	**0.74**	0.52	**0.65**	**0.58**
	alkylated PAHs	0.01	**0.75**	-0.16	-0.26	0.21	0.29	0.01	0.24	0.09	0.14
	alkanes	-0.10	0.31	-0.19	-0.38	-0.17	-0.12	-0.25	-0.10	-0.22	-0.17
	alkanols	-0.11	0.26	0.43	**0.70**	0.22	0.17	0.36	0.06	0.35	0.38
	anhydrous sugars	0.53	-0.24	**0.70**	0.35	**0.68**	**0.61**	**0.71**	**0.65**	**0.78**	**0.76**
	guaiacyls	0.10	0.26	0.10	-0.09	0.29	0.30	0.21	0.26	0.28	0.28
	nitrophenols	-0.17	-0.14	**0.60**	**0.76**	0.09	-0.03	0.37	-0.08	0.32	0.31
	resin acids	**0.63**	0.23	-0.24	-0.42	0.45	0.54	0.09	**0.66**	0.25	0.24
	polyols	0.27	-0.09	**0.93**	**0.63**	**0.71**	**0.61**	**0.89**	0.51	**0.87**	**0.87**
	dicarboxylic acids	0.12	-0.01	**0.87**	**0.74**	**0.63**	0.53	**0.83**	0.40	**0.80**	**0.81**
	multifunctional acids/anhydrids	-0.10	-0.16	**0.93**	**0.89**	0.40	0.26	**0.71**	0.15	**0.66**	**0.67**
	fatty acids	-0.05	0.50	-0.40	-0.34	-0.08	0.01	-0.26	-0.01	-0.21	-0.15

References

Atkinson, R., Baulch, D. L., Cox, R. A., Crowley, J. N., Hampson Jr, R. F., Kerr, J. A., Rossi, M. J. and Troe, J.: Summary of evaluated kinetic and photochemical data for atmospheric chemistry, IUPAC Subcommittee on gas kinetic data evaluation for atmospheric chemistry, 20, 2001.

Atkinson, R.: Kinetics and mechanisms of the gas-phase reactions of the hydroxyl radical with organic compounds under atmospheric conditions, Chem. Rev., 86, 69-201, 1986.

Atkinson, R., Aschmann, S. M. and Carter, W. P.: Kinetics of the reactions of O3 and OH radicals with furan and thiophene at 298±2 K, Int J Chem Kinet, 15, 51-61, 1983.

Avagyan, R., Nyström, R., Lindgren, R., Boman, C. and Westerholm, R.: Particulate hydroxy-PAH emissions from a residential wood log stove using different fuels and burning conditions, Atmos. Environ., 140, 1-9, 2016.

Barmet, P., Dommen, J., DeCarlo, P. F., Tritscher, T., Praplan, A. P., Platt, S. M., Prévôt, A. S. H., Donahue, N. M. and Baltensperger, U.: OH clock determination by proton transfer reaction mass spectrometry at an environmental chamber, Atmos. Meas. Tech., 5, 647, 2012.

Baulch, D. L., Cobos, C. J., Cox, R. A., Frank, P., Hayman, G., Just, T., Kerr, J. A., Murrells, T., Pilling, M. J., Troe, J., Walker, W. and Warnatz, J.: Evaluated kinetic data for combustion modeling. Supplement I, J. Phys. Chem. Ref. Data, 23, 847-848, 1994.

Baulch, D. L., Cobos, C., Cox, R. A., Esser, C., Frank, P., Just, T., Kerr, J. A., Pilling, M. J., Troe, J. and Walker, R. W., and Warnatz, J.: Evaluated kinetic data for combustion modelling, J. Phys. Chem. Ref. Data, 21, 411-734, 1992.

Bertrand, A., Stefenelli, G., Jen, C. N., Pieber, S. M., Bruns, E. A., Ni, H., Temime-Roussel, B., Slowik, J. G., Goldstein, A. H., El Haddad, I., Baltensperger, U., Prévôt, A. S. H., Wortham, H. and Marchand, N.: Evolution of the chemical fingerprint of biomass burning organic aerosol during aging, Atmos. Chem. Phys., 18, 7607-7624, 2018.

Bruns, E. A., Krapf, M., Orasche, J., Huang, Y., Zimmermann, R., Drinovec, L., Močnik, G., El-Haddad, I., Slowik, J. G., Dommen, J., Baltensperger, U. and Prévôt, A S H: Characterization of primary and secondary wood combustion products generated under different burner loads, Atmos. Chem. Phys., 15, 2825-2841, 2015.

Cappellin, L., Karl, T., Probst, M., Ismailova, O., Winkler, P. M., Soukoulis, C., Aprea, E., Märk, T. D., Gasperi, F. and Biasioli, F.: On quantitative determination of volatile organic compound concentrations using proton transfer reaction time-of-flight mass spectrometry, Environ. Sci. Technol., 46, 2283-2290, 2012.

Cvetanović, R. J.: Evaluated chemical kinetic data for the reactions of atomic oxygen O (3P) with unsaturated hydrocarbons, J. Phys. Chem. Ref. Data, 16, 261-326, 1987.

Czech, H., Miersch, T., Orasche, J., Abbaszade, G., Sippula, O., Tissari, J., Michalke, B., Schnelle-Kreis, J., Streibel, T., Jokiniemi, J. and Zimmermann, R.: Chemical composition and speciation of particulate organic matter from modern residential small-scale wood combustion appliances, Sci. Total Environ., 612, 636-648, 2018.

Grosjean, E. and Grosjean, D.: Rate constants for the gas-phase reaction of ozone with 1, 1-disubstituted alkenes, Int J Chem Kinet, 28, 911-918, 1996.

Hartikainen, A., Yli-Pirilä, P., Tiitta, P., Leskinen, A., Kortelainen, M., Orasche, J., Schnelle-Kreis, J., Lehtinen, K. E., Zimmermann, R., Jokiniemi, J. and Sippula O.: Volatile organic compounds from logwood combustion: emissions and transformation under dark and photochemical aging conditions in a smog chamber, Environ. Sci. Technol., 52, 4979-4988, 2018.

Herron, J. T.: Evaluated chemical kinetic data for the reactions of atomic oxygen O(3P) with saturated organic compounds in the gas phase, J. Phys. Chem. Ref. Data, 17, 967-1026, 1988.

Herring, C. L., Faiola, C. L., Massoli, P., Sueper, D., Erickson, M. H., McDonald, J. D., Simpson, C. D., Yost, M. G., Jobson, B. T. and VanReken, T. M.: New methodology for quantifying polycyclic aromatic hydrocarbons (PAHs) using high-resolution aerosol mass spectrometry, Aerosol Sci. Tech., 49, 1131-1148, 2015.

Keller-Rudek, H., Moortgat, G. K., Sander, R. and Sörensen, R.: The MPI-Mainz UV/VIS Spectral Atlas of Gaseous Molecules of Atmospheric Interest, [online] Available from: www.uv-vis-spectral-atlas-mainz.org, 2015.

Kroll, J. H., Donahue, N. M., Jimenez, J. L., Kessler, S. H., Canagaratna, M. R., Wilson, K. R., Altieri, K. E., Mazzoleni, L. R., Wozniak, A. S., Bluhm, H., Mysak, E. R., Smith, J. D., Kolb, C. E. and Worsnop, D. R.: Carbon oxidation state as a metric for describing the chemistry of atmospheric organic aerosol, Nat. Chem., 3, 133, 2011.

Lehtinen, K. E., Korhonen, H., Maso, M. D. and Kulmala, M.: On the concept of condensation sink diameter, Boreal Environ. Res., 8, 405-412, 2003.

Li, R., Palm, B. B., Ortega, A. M., Hlywiak, J., Hu, W., Peng, Z., Day, D. A., Knote, C., Brune, W. H., De Gouw, J. A. and Jimenez, J. L.: Modeling the radical chemistry in an oxidation flow reactor: radical formation and recycling, sensitivities, and the OH exposure estimation equation, The Journal of Physical Chemistry A, 119, 4418-4432, 2015.

Manion, J.A., Huie, R. E., Levin, R. D., Burgess Jr., D. R., Orkin, V. L., Tsang, W., McGivern, W. S., Hudgens, J. W., Knyazev, V. D., Atkinson, D. B., Chai, E., Tereza, A. M., Lin, C.-Y., Allison, T. C., Mallard, W. G., Westley, F., Herron, J. T., Hampson, R. F., and Frizzell, D. H., NIST Chemical Kinetics Database, NIST Standard Reference Database 17, Version 7.0 (Web Version), Release 1.6.8, Data version 2015.09, National Institute of Standards and Technology, Gaithersburg, Maryland, 20899-8320. Web address: http://kinetics.nist.gov/

Miersch, T., Czech, H., Hartikainen, A., Ihalainen, M., Orasche, J., Abbaszade, G., Tissari, J., Streibel, T., Jokiniemi, J., Sippula, O. and Zimmermann, R.: Impact of photochemical ageing on Polycyclic Aromatic Hydrocarbons (PAH) and oxygenated PAH (Oxy-PAH/OH-PAH) in logwood stove emissions, Sci. Total Environ., 686, 382-392, 2019.

Orasche, J., Schnelle-Kreis, J., Abbaszade, G. and Zimmermann, R.: In-situ derivatization thermal desorption GC-TOFMS for direct analysis of particle-bound non-polar and polar organic species, Atmos. Chem. Phys., 11, 8977-8993, 2011.

Palm, B. B., Campuzano-Jost, P., Ortega, A. M., Day, D. A., Kaser, L., Jud, W., Karl, T., Hansel, A., Hunter, J. F., Cross, E. S., Kroll, J. H., Peng, Z., Brune, W. H. and Jimenez, J. L.: In situ secondary organic aerosol formation from ambient pine forest air using an oxidation flow reactor, Atmos. Chem. Phys., 16, 2943-2970, 2016.

Paulson, S. E., Orlando, J. J., Tyndall, G. S. and Calvert, J. G.: Rate coefficients for the reactions of O (3P) with selected biogenic Hydrocarbons, Int J Chem Kinet, 27, 997-1008, 1995.

Peng, Z., Day, D. A., Ortega, A. M., Palm, B. B., Hu, W., Stark, H., Li, R., Tsigaridis, K., Brune, W. H. and Jimenez, J. L.: Non-OH chemistry in oxidation flow reactors for the study of atmospheric chemistry systematically examined by modeling, Atmos. Chem. Phys., 16, 4283-4305, 2016.

Peng, Z. and Jimenez, J. L.: Modeling of the chemistry in oxidation flow reactors with high initial NO, Atmos. Chem. Phys., 17, 11991-12010, 2017.

Peng, Z., Lee-Taylor, J., Orlando, J. J., Tyndall, G. S. and Jimenez, J. L.: Organic peroxy radical chemistry in oxidation flow reactors and environmental chambers and their atmospheric relevance, Atmospheric Chem. Phys., 19(2), 813–834, doi:10.5194/acp-19-813-2019, 2019.

Stedman, D. H. and Niki, H.: Ozonolysis rates of some atmospheric gases, Environ. Lett., 4, 303-310, 1973.

Tang, M. J., Shiraiwa, M., Pöschl, U., Cox, R. A. and Kalberer, M.: Compilation and evaluation of gas phase diffusion coefficients of reactive trace gases in the atmosphere: Volume 2. Diffusivities of organic compounds, pressure-normalised mean free paths, and average Knudsen numbers for gas uptake calculations, Atmos. Chem. Phys., 15, 5585-5598, 2015.

Toby, S., Van de Burgt, L J and Toby, F. S.: Kinetics and chemiluminescence of ozone-aromatic reactions in the gas phase, J. Phys. Chem., 89, 1982-1986, 1985.